BBA - Molecular Basis of Disease 1863 (2017) 3038–3048

Contents lists available at ScienceDirect

BBA - Molecular Basis of Disease

journal homepage: www.elsevier.com/locate/bbadis

Structural determinants in ApoA-I amyloidogenic variants explain improved cholesterol metabolism despite low HDL levels

Rita Del Giudice[a,*], Joan Domingo-Espín[a], Ilaria Iacobucci[b,c], Oktawia Nilsson[a], Maria Monti[b,d], Daria Maria Monti[b,d], Jens O. Lagerstedt[a,*]

[a] Department of Experimental Medical Science, Lund University, 221 84 Lund, Sweden
[b] Department of Chemical Sciences, University of Naples Federico II, 80126 Naples, Italy
[c] CEINGE Biotecnologie Avanzate, 80145 Naples, Italy
[d] Istituto Nazionale di Biostrutture e Biosistemi (INBB), Rome, Italy

ARTICLE INFO

Keywords:
Apolipoprotein A-I
Amyloidosis
High-density lipoprotein
Hypoalphalipoproteinemia
Cholesterol efflux

ABSTRACT

Twenty Apolipoprotein A-I (ApoA-I) variants are responsible for a systemic hereditary amyloidosis in which protein fibrils can accumulate in different organs, leading to their failure. Several ApoA-I amyloidogenic mutations are also associated with hypoalphalipoproteinemia, low ApoA-I and high-density lipoprotein (HDL)-cholesterol plasma levels; however, subjects affected by ApoA-I-related amyloidosis do not show a higher risk of cardiovascular diseases (CVD). The structural features, the lipid binding properties and the functionality of four ApoA-I amyloidogenic variants were therefore inspected in order to clarify the paradox observed in the clinical phenotype of the affected subjects.

Our results show that ApoA-I amyloidogenic variants are characterized by a different oligomerization pattern and that the position of the mutation in the ApoA-I sequence affects the molecular structure of the formed HDL particles. Although lipidation increases ApoA-I proteins stability, all the amyloidogenic variants analyzed show a lower affinity for lipids, both *in vitro* and in *ex vivo* mouse serum. Interestingly, the lower efficiency at forming HDL particles is compensated by a higher efficiency at catalysing cholesterol efflux from macrophages.

The decreased affinity of ApoA-I amyloidogenic variants for lipids, together with the increased efficiency in the cholesterol efflux process, could explain why, despite the unfavourable lipid profile, patients affected by ApoA-I related amyloidosis do not show a higher CVD risk.

1. Introduction

Apolipoprotein A-I (ApoA-I) hereditary systemic amyloidosis is a rare, autosomal dominant, late onset disease caused by specific mutations in the APOA1 gene [1]. The disease is characterized by the progressive accumulation of protein fibrils in the affected organs, such as heart, liver, kidneys, nerves, ovaries or testes, eventually leading to organ failure [2–4].

ApoA-I represents the major protein component of high density lipoprotein (HDL) and plays a fundamental role in lipid metabolism, both in delivering cholesterol to steroidogenic tissues and in transporting it from the periphery to the liver for catabolism in the process known as reverse cholesterol transport (RCT) [5]. To exert its functions in the RCT, lipid free/poor ApoA-I interacts with the ATP binding cassette A1 (ABCA1) in peripheral tissues to promote the efflux of cholesterol from macrophages, thus forming nascent HDL particles. These particles become mature after the esterification of cholesterol through lecithin:cholesterol acyltransferase (LCAT). Maturation of spherical HDL is a necessary step to allow the interaction of ApoA-I with the scavenger receptor class B type 1 (SRB1), present on the hepatocytes, to release cholesterol [6]. Therefore, ApoA-I plays an anti-atherogenic role, protecting against cardiovascular diseases (CVD) [7,8].

ApoA-I is mainly associated to lipids but it can also be found in a lipid-free state (5–10%) [9]. In healthy subjects, serum lipid free ApoA-I can either form new HDL particles, or bind to existing ones, or can be catabolized [5,10]. In the presence of one of the twenty amyloidogenic

Abbreviations: ABCA1, ATP binding cassette A1; ApoA-I, apolipoprotein A-I; CVD, cardiovascular disease; DLS, dynamic light scattering; DMPC, 1,2-dimyristoyl-sn-glycero-3-phosphocholine; HDL, high-density lipoprotein; LB, lipid bound; LCAT, lecithin:cholesterol acyltransferase; LF, lipid free; PBS, phosphate buffer saline; POPC, 1-palmitoyl-2-oleoyl-sn-glycero-3-phosphocholine; RCT, reverse cholesterol transport; rHDL, reconstituted HDL; SRB1, scavenger receptor class B type 1; SRCD, synchrotron radiation circular dichroism; TEV, tobacco etch virus; WT, wild-type

* Corresponding authors.
E-mail addresses: rita.del_giudice@med.lu.se (R. Del Giudice), jens.lagerstedt@med.lu.se (J.O. Lagerstedt).

http://dx.doi.org/10.1016/j.bbadis.2017.09.001
Received 1 June 2017; Received in revised form 30 August 2017; Accepted 1 September 2017
Available online 06 September 2017

mutations identified so far, lipid-free ApoA-I can also face an alternative fate, where misfolding of the protein leads to aggregation in amyloid fibrils [11,12]. Although the molecular mechanism of fibril formation and accumulation of ApoA-I amyloidogenic variants has been extensively studied [13–18], it remains not fully understood. Interestingly, the localization of the mutations in the ApoA-I protein sequence seems to direct protein aggregation in specific organs. Indeed, amyloidogenic mutations in the residues 1–75 of the protein lead mostly to hepatic, renal, and testis amyloidosis, whereas mutations in residues 173 to 178 mainly lead to cardiac, laryngeal, and cutaneous protein accumulation [2,3]. The determinants of this tissue-specificity currently represent a challenge in the study of ApoA-I-related amyloidosis.

Some ApoA-I amyloidogenic variants have been found associated with hypoalphalipoproteinemia and with a reduction of plasma ApoA-I levels. In subjects carrying the substitution of a glycine in position 26 with an arginine (G26R variant), the lower plasma levels of HDL and ApoA-I were found to be a consequence of an accelerated metabolism of both the mutated and the native protein [19]. In two clinical studies, involving 30 and 253 affected individuals respectively, carriers of the amyloidogenic variant with leucine to proline substitution at position 75 (L75P variant) displayed lower levels of plasma ApoA-I, decreased levels of HDL (32% decrease relative to healthy subject) and significant reduction in HDL-cholesterol [4,20]. Similarly, a clinical case study conducted on a subject carrying the ApoA-I variant with a leucine to serine substitution in position 174 (L174S variant), showed a significant reduction of serum ApoA-I and HDL- and total cholesterol compared to the healthy relatives [21]. Interestingly, despite this unfavourable lipid profile, patients affected by ApoA-I-related systemic amyloidosis do not show a significant higher risk of cardiovascular diseases, as recently demonstrated in a clinical study on 131 carriers of the L75P variant. In this study, Muiesan and co-workers found that L75P carriers do not show any structural and functional vascular abnormality, allowing them to hypothesize that the low levels of HDL and HDL-cholesterol observed in the affected subjects is balanced by a still unclear “protective” mechanism [22].

In order to shed light on the structural and functional disparities among the different variants, we focused on four ApoA-I amyloidogenic variants, of which two accumulate preferentially in the liver and kidney (G26R and L75P), and two are known to form fibrils preferentially in heart and skin (L174S and L178H), as well as the wild-type protein [23–26]. These amyloidogenic variants are also representative of the two hot-spot mutation sites present in the crystal structure of the C-terminal truncated version of the protein [27,28]. For the first time, our findings define a connection between the alterations in the protein structure and function and the clinical phenotype.

2. Materials and methods

2.1. Production of recombinant ApoA-I amyloidogenic variants

ApoA-I amyloidogenic variants, as well as the WT protein, were produced in a bacterial expression system consisting of ApoA-I expressing pEXP-5 plasmid in *Escherichia coli* strain BL21(DE3) pLysS (Invitrogen), as previously described [14,29] with some modifications. Primer-directed PCR mutagenesis was used to introduce the G26R, L75P, L174S and L178H mutations and the constructs were verified by dideoxy automated fluorescent sequencing (GATC Biotech). Bacterial cells were transformed with recombinant plasmids and cultivated in Luria Bertani medium at 37 °C, for the production of WT and L178H variant, in NZYM with 0.2% glucose at 37 °C or 30 °C, for the production of G26R and L174S variants respectively, and in EnPresso® B medium (BioSilta), at 30 °C, for the production of L75P variant. All the media were supplemented with 50 μg/ml ampicillin and 34 μg/ml chloramphenicol. Protein expression was induced for 4 h following the addition of 1 mM isopropyl-beta-thiogalactopyranoside (Thermo). His-tagged ApoA-I variants were purified from bacterial cell lysate by immobilized metal affinity chromatography (His-Trap-Nickel-chelating columns, GE Healthcare) under denaturing conditions (3 M guanidine in phosphate-buffered saline (PBS), pH 7.4). Following binding, an extensive wash with 40 mM imidazole in PBS was performed and bound proteins were then eluted with 500 mM imidazole in PBS. Imidazole was removed from protein samples by using desalting columns (GE Healthcare) equilibrated with PBS, pH 7.4, and tobacco etch virus (TEV) protease was employed overnight at 4 °C to remove the His-tag from protein samples. At the end of the incubation, a second Ni^{2+}-column step was employed in order purify the cleaved ApoA-I from TEV protease and the His-tag, with the latter two being retained on the column. The flow-through, containing cleaved ApoA-I variants, was desalted in PBS, pH 7.4, concentrated with 10 kDa cut-off Amicon Ultra centrifugal filters (Millipore) and stored at 4 °C prior to use. Protein concentration was determined by Nanodrop and protein purity was confirmed by sodium dodecyl sulfate (SDS)-polyacrylamide gel electrophoresis with Coomassie blue staining.

2.2. Lipidation of ApoA-I amyloidogenic variants

2.2.1. DMPC lipoparticles preparation

Lyophilized DMPC (1,2-dimyristoyl-sn-glycero-3-phosphocholine; Avanti Polar Lipids) was dissolved in 3:1 chloroform:methanol and the solvent was completely evaporated by overnight incubation under a stream of nitrogen gas. DMPC was then dissolved in PBS or McIlvaine buffer (165 mM Na_2HPO_4, 17.6 mM citrate, pH 7.0) and the lipid suspension was extruded through a 100-nm polycarbonate membrane using the LiposoFast system (Avestin) to create multilamellar vesicles. The reconstituted HDL particles (rHDLs) were produced by incubating the recombinant proteins with multilamellar DMPC particles at a 1:100 protein to lipid molar ratio and a protein concentration of 1 mg/ml at 24 °C, the transition temperature for DMPC, for 96 h.

2.2.2. POPC lipoparticles preparation

Lyophilized POPC (1-palmitoyl-2-oleoyl-sn-glycero-3-phosphocholine, Avanti Polar Lipids) was dissolved in 3:1 chloroform:methanol and the solvent evaporated by overnight incubation under a stream of nitrogen gas. POPC was dissolved in PBS and lipoparticles were generated by using the cholate dialysis method. Briefly, POPC lipoparticles were produced by incubating ApoA-I proteins with a mixture of 1:2 POPC:sodium deoxycolate at a 1:80 protein to lipid molar ratio at a 0.5 mg/ml protein concentration. Mixtures were incubated at 37 °C for 1 h and then dialysed against PBS for 72 h.

At the end of the incubation, rHDLs (both DMPC and POPC particles) were analyzed by Blue Native PAGE by using the NativePAGE Bis-Tris Gel System 4–16% (Invitrogen) according to the manufacturer's instructions.

2.2.3. Lipid clearance assay

Lipid clearance was monitored by monitoring the decrease in the absorbance of the multilamellar vesicles and protein mixture at 325 nm every 10 s for 10 min, as previously described [29].

2.2.4. Formation of rHDL in vitro

Amyloidogenic ApoA-I variants, as well as the WT protein, were mixed with DMPC multilamellar vesicles (1:100 protein to lipid molar ratio) at the concentration of 0.4 mg/ml and incubated at 24 °C, in agitation. Samples were taken at 0, 1, 3, 6, 9, 12, 24, 96 h and stored at − 80 °C in the presence of 10% sucrose prior the Blue Native PAGE analysis or analyzed by Synchrotron Radiation Circular Dichroism (SRCD) directly at the end of each incubation time.

2.2.5. Formation of rHDL ex vivo

Male C57BL/6 mice were purchased from Taconic (Ry, Denmark) and were used at the age of 8 weeks. The protocol for the rHDL formation *ex vivo* was adapted from [29]. Briefly, blood samples were

collected by cardiac puncture and serum samples (200 μl) were mixed with ApoA-I amyloidogenic variants and the WT protein at the concentration of 0.75 mg/ml. The mixtures were incubated at 37 °C, in agitation, samples were taken after 0, 0.5, 1, 3, 6, 9, 24 and 48 h and stored at − 80 °C. The samples were separated by NativePAGE Bis-Tris Gels System 4–16% (Invitrogen), transferred to PVDF membranes, and probed with anti-human ApoA-I antibodies (ab64308, Abcam). Detection was performed by using HRP-conjugated secondary antibodies (GE Healthcare) and a chemi-luminescence detection substrate (SuperSignal® West Femto, Thermo Scientific). Blots were imaged using the Odyssey Fc system (LI-COR).

The animal procedures were approved by the Malmö/Lund Committee for Animal Experiment Ethics.

2.3. Dynamic light scattering

Volume-size distribution of lipid-free and -bound proteins was determined by using a Malvern Zetasizer Nano (Malvern Instruments Limited), using plastic cuvettes with a final volume of 60 μL. Protein samples were diluted at 0.5 mg/ml in McIlvaine buffer and centrifuged at 14000 rpm for 30 min. Data was processed using Zetasizer family software version 7.11 (Malvern Instruments Limited). All quality information was reported as good and therefore accepted.

2.4. Synchrotron radiation circular dichroism

SRCD experiments were performed using a nitrogen-flushed Module B end-station spectrophotometer at B23 Synchrotron Radiation CD Beamline at the Diamond Light Source, Oxfordshire, UK [30,31]. The data were analyzed using CDApps [32] and the estimation of secondary structure was performed using the CONTINLL algorithm [33] with reference data SP 43, between 190 and 260 nm.

2.4.1. Concentration dependence studies

Lipid free (LF) ApoA-I protein samples were dialysed against McIlvaine buffer in order to minimize the noise at wavelengths below 200 nm. Protein samples were diluted at 0.1, 0.5 and 1.5 mg/ml, loaded into quartz cuvettes (0.1, 0.2 or 0.5 mm path lengths, depending on protein concentration) and the spectra acquired at 25 °C in the far-UV range 185–260 nm, with a 1 nm wavelength increment. All the spectra were corrected subtracting the background signal of the buffer.

2.4.2. rHDL particles analysis

rHDL particles (lipid-bound (LB) samples) were produced in McIlvaine buffer and analyzed by SRCD at 0.5 mg/ml in a 0.2 nm quartz cuvette. Spectra were acquired at 24 °C in the far-UV range 185–260 nm, with a 1 nm wavelength increment. All the spectra were corrected subtracting the background signal of DMPC vesicles diluted in McIlvain buffer.

2.4.3. Thermal stability analyses of LB proteins

LB samples were diluted in McIlvaine buffer at 0.5 mg/ml and placed in a 0.2 mm quartz cuvette. SRCD spectra were collected in 25–85 °C range, with a 10 °C increment. The analysis of the secondary structure during the thermal denaturation was performed by using the CONTINLL algorithm with reference data SP 43, between 190 and 260 nm.

2.5. Complementary proteolysis experiments and mass spectrometry analysis

LB and LF ApoA-I proteins (0.3 mg/ml) were treated with trypsin, chymotrypsin, endoproteinase Glu-C and subtilisin in PBS, pH 7.4. Each enzyme:substrate (E:S) ratio was optimized for each proteolytic probe on the LF and LB WT ApoA-I and the same amount of enzyme was employed to digest all ApoA-I variants. For the experiments on LF proteins, the E:S employed were 1:8000 for chymotrypsin and trypsin, 1:10,000 for Glu-C and subtilisin, whereas for LB samples the E:S were 1:3000 for chymotrypsin, 1:100 for trypsin, 1:200 for Glu-C and 1:1000 for subtilisin. Digestions were monitored on a time-course basis by sampling the reaction products at different times (15 and 30 min, or 30 and 60 min) and blocking enzyme digestions with 2% trifluoroacetic acid (TFA). Peptide mixtures from the different proteolysis experiments were analyzed by liquid chromatography-mass spectrometry (LC-MS) onto a Quattro Micro LC-MS system (Micromass, Waters) coupled with a 1100 HPLC (Agilent Technologies, Palo Alto, CA). Peptides fractionations were carried out by reverse-phase HPLC on a Phenomenex Jupiter C18 column (250 mm × 2.1 mm, 300 Å pore size) and eluted by using a step gradient from 5% to 60% of solvent B (5% formic acid and 0.05% TFA in acetonitrile) over 60 min and from 60% to 95% in 5 min (solvent A 5% formic acid and 0.05% TFA in water), at flow rate of 200 μl/min directly introduced in mass spectrometers ESI source. Horse heart myoglobin (average molecular mass 16,951.5 Da) was used as standard for the instrument calibration at 5 scans/s.

2.6. Cholesterol efflux

Cholesterol efflux assay was adapted from [29,34,35] with some modifications. J774 macrophages (ATCC, TIB-67) were plated into 24-well cell culture dishes at 100,000 cells/well in RPMI 1640 (Gibco) supplemented with 10% FBS and 50 μg/ml gentamicin. 24 h after plating, the medium was replaced with RPMI 1640 containing 5% FBS, 4 μCi/ml ^{3}H-cholesterol (Perkin Elmer), 2 μg/ml ACAT inhibitor (Sandoz 58–035, Sigma) and 50 μg/ml gentamicin. After a further 24 h incubation, the medium was replaced with RPMI 1640 supplemented with 0.2% BSA (low free fatty acids and low endotoxin, Sigma), 2 μg/ml ACAT inhibitor, 0.3 mM Cpt-cAMP (Abcam) and 50 μg/ml gentamicin for 18 h. At the end of incubation, cells were washed twice with RPMI 1640 and then triplicate wells were treated with the amyloidogenic variants or the WT protein, both in their LF or LB form (either DMPC- or POPC-ApoA-I particles), in RPMI 1640 supplemented with 0.2% BSA, at the indicated concentrations for 2, 4 or 24 h. Cholesterol efflux was measured in the media by centrifugation at 4000 × *g* for 5 min at room temperature and transfer of 100 μl supernatant to a scintillation vial. 5 ml of scintillation fluid was added to each sample before scintillation counting was performed (Perkin Elmer). The measure of the total ^{3}H-cholesterol in the cells was obtained by solubilizing the incubated cells, in triplicate, with 1% sodium deoxycholate and scintillation counting of the collected lysates. Efflux for each treatment was calculated as the percentage of the total ^{3}H-cholesterol. Non-specific background efflux was measured in triplicate for each time point, in each experiment, and the efflux for each treatment subtracted for this value.

2.7. Statistical analysis

Data shown are the mean ± SD or ± SEM, as indicated. Analysis was performed by one-way ANOVA with Tukey's *post hoc* test, using the GraphPad software.

3. Results

3.1. ApoA-I amyloidogenic variants' secondary structure is influenced by protein concentration and association with lipids

To explore the structural disparities among the ApoA-I amyloidogenic variants, protein samples were analyzed in their lipid free (LF) and lipid bound (LB) states, by using several biophysical approaches (Fig. 1).

LF proteins were analyzed by Blue Native Gel electrophoresis and dynamic light scattering (DLS) (Fig. 1a). As shown in the Native Gel, all proteins presented a pattern composed of two species, a less abundant one, approximately of 7.8 nm, and a predominant one with a smaller

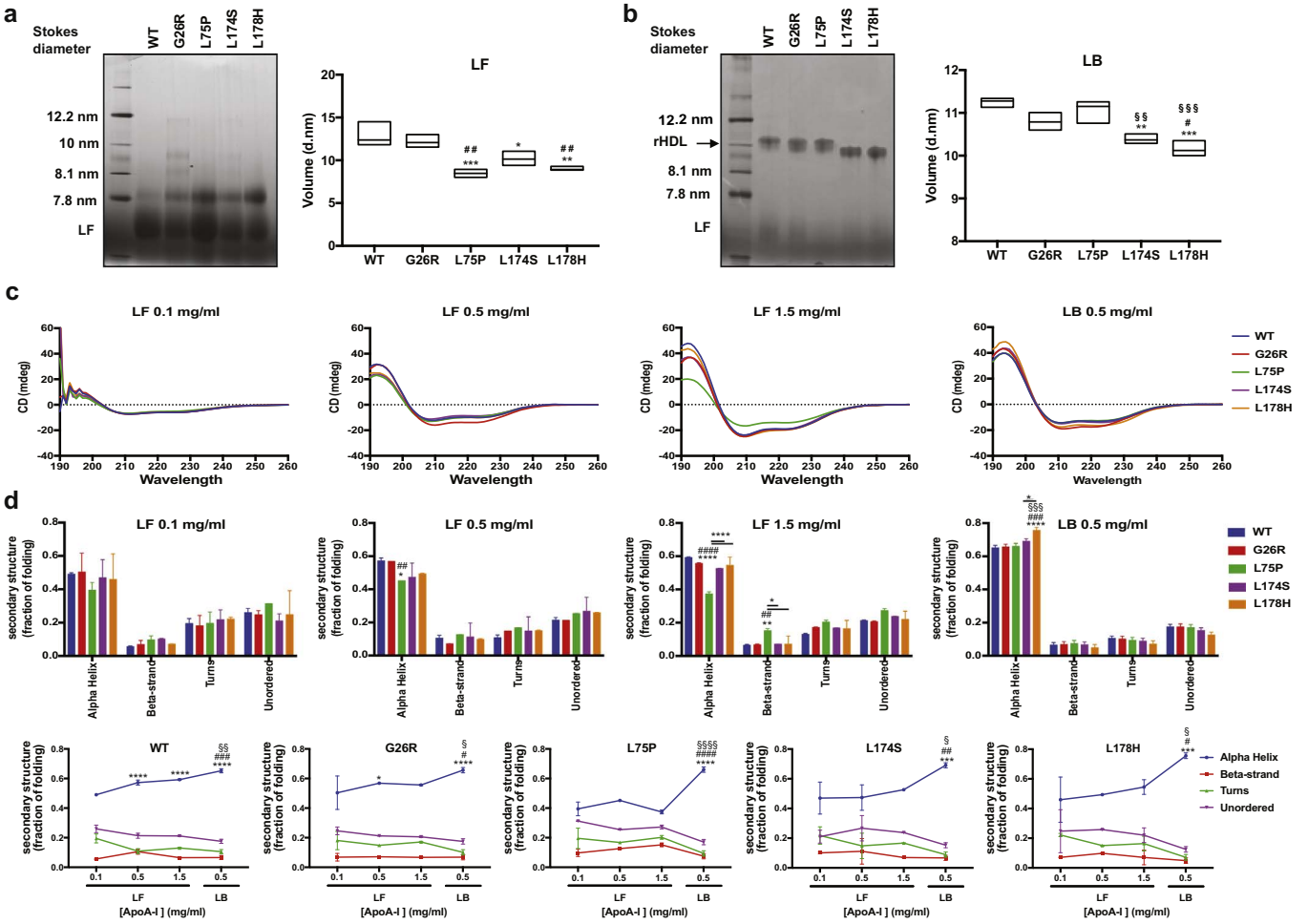

Fig. 1. ApoA-I variants' secondary structure depends on protein concentration and lipidation state. Blue Native gels and DLS analysis of (**a**) lipid free (LF) or (**b**) lipid bound (LB) ApoA-I amyloidogenic variants. Gels were loaded with 5 μg of each protein. The LB proteins were obtained by incubating the ApoA-I variants, as well as the WT protein, with DMPC multilamellar vesicles at 24 °C for 96 h. Data shown represents the contribution of the experimental data with a line at the median ($n = 3$). Significance is calculated according to one-way ANOVA ($^{*}p < 0.05$, $^{***}p < 0.001$ for groups as shown with respect to the WT protein, $^{\#}p < 0.05$, $^{\#\#}p < 0.01$ for groups as shown with respect to G26R, $^{\S\S}p < 0.005$, $^{\S\S\S}p < 0.001$, for groups as shown with respect to L75P variant). (**c**) SRCD spectra of LF proteins at different concentrations (0.1, 0.5 and 1.5 mg/ml) and LB proteins at 0.5 mg/ml. (**d**) Secondary structure estimation of ApoA-I amyloidogenic variants, obtained by analysing the spectra in (**c**) with the CONTINLL algorithm. Data shown are the mean ± SD (n = 3 for LF 0.1 mg/ml and $n = 2$ for the other protein samples). Significance is calculated according to two-way ANOVA. Upper panel, $^{*}p < 0.05$, $^{**}p < 0.005$, $^{****}p < 0.0001$ for groups as shown with respect to the WT protein, $^{\#\#}p < 0.005$, $^{\#\#\#}p < 0.00$, $^{\#\#\#\#}p < 0.0001$ for groups as shown with respect to G26R variant, $^{\S\S\S}p < 0.001$ for groups as shown with respect to L75P variant. Lower panel, $^{*}p < 0.05$, $^{***}p < 0.001$, $^{****}p < 0.0001$ for groups as shown with respect 0.1 mg/ml, $^{\#}p < 0.05$, $^{\#\#}p < 0.005$, $^{\#\#\#}p < 0.00$, $^{\#\#\#\#}p < 0.0001$ for groups as shown with respect to LF 0.5 mg/ml, $^{\S}p < 0.05$, $^{\S\S}p < 0.005$, $^{\S\S\S\S}p < 0.0001$ for groups as shown with respect to 1.5 mg/ml.

size. In particular, in the case of L75P and L178H variants the 7.8 nm species was more abundant compared to the WT. Interestingly, the G26R and L174S variants presented three other species of higher sizes (8.1, 9 and 12.2 nm, approximately), particularly evident in the case of G26R variant. However, for G26R variant, the estimated averaged hydrodynamic diameter, obtained by DLS, was found to be very similar to that determined for the native protein (12.9 and 12.2 nm for WT and G26R, respectively), whereas the other variants showed significantly lower diameters (8.5, 9.0 and 10.2 nm for L75P, L174S and L178H, respectively). Although these results are in good agreement with those previously obtained on the native and L174S variant [17], the hydrodynamic diameter observed here for the lipid-free L75P variant is significantly smaller.

Then, reconstituted HDL particles (herein referred to as rHDLs or LB) were produced by incubating the recombinant proteins with multilamellar DMPC particles at a 1:100 protein to lipid molar ratio and a protein concentration of 0.5 mg/ml at 24 °C, which is the transition temperature for DMPC. After 4 days of incubation, the rHDLs were analyzed by native gel electrophoresis (Fig. 1b). It is worth to notice that, although the Stokes diameter of all the rHDLs was found to be approximately 10 nm, the particles formed by the L174S and L178H variants showed a slightly smaller size with respect to those produced by G26R and L75P variants as well as the WT protein, suggesting that the position of the amyloidogenic mutation in the ApoA-I sequence could alter the molecular structure of the formed rHDLs. These results are in good agreement with those obtained by DLS. Indeed, as shown in Fig. 1b, right panel, the hydrodynamic volume calculated for the L174S and L178H variants was significantly smaller (10.4 and 10.2 nm for L174S and L178H, respectively) compared to that calculated for the WT protein and the other ApoA-I variants (11.3, 10.8 and 11.1 nm for WT, G26R and L75P, respectively).

Then, the secondary structure of all ApoA-I variants was investigated by far-UV synchrotron radiation circular dichroism (SRCD) spectroscopy (Fig. 1c–d). SRCD spectroscopy was chosen as the high photon flux that characterize the synchrotron light enables measurements of proteins in the presence of highly interfering molecules such as phospholipids. The decrease of the noise in the 180–200 nm spectral range made then possible the estimation of the secondary structure content of the ApoA-I proteins in their lipid bound state.

First, the impact of protein oligomerization on the proteins'

secondary structure was analyzed as a function of protein concentration. In Fig. 1c, representative spectra of the ApoA-I variants at different concentration (0.1, 0.5 and 1.5 mg/ml, representing different oligomeric states of the ApoA-I proteins) and in their lipid bound state (0.5 mg/ml) are reported. As shown in Fig. 1d, the increase of protein concentration led to an increase in the α-helical content with a concomitant reduction in turns and unordered content. This trend was particularly evident for the WT and the G26R variant in which the α-helical content increased from about 50% at 0.1 mg/ml to about 60% at 1.5 mg/ml. The L174S and L178H variants showed a similar behavior but the major increase in the α-helical content occurred when the protein concentration was increased from 0.5 mg/ml to 1.5 mg/ml (from about 48% at 0.5 mg/ml to about 54% at 1.5 mg/ml). Interestingly, the L75P variant (Fig. 1c–d,) did not follow the same trend, as the α-helical content for this variant remained approximately 40%, and the increase in protein concentration led to a higher β-strand content (from 10 to 15%). These results suggest that, even though ApoA-I conformation and oligomeric state are generally dependent on protein concentration, the extent of structural rearrangements might be affected by the position of the mutation in the protein sequence.

Then, the effects of lipidation on ApoA-I variants' secondary structure was evaluated. In their lipid bound state (Fig. 1c–d, right panels), all the proteins acquired a predominant α-helical conformation. Notably, although the L75P variant showed the lower α-helical content in its lipid free state, the HDL-bound L75P variant acquired a secondary structure conformation very close to that of the WT protein. L174S- and L178H-HDLs also showed an interesting behavior since they were characterized by a higher helicity (70% and 76%, respectively) compared to the G26R and L75P variants, and the WT protein (all having about 65% α-helical content), as well as a decrease in unordered and turns. The differences observed in the secondary structure contents and, in particular, in the α-helix content, could explain the difference in the size of the lipoparticles prepared with the different amyloidogenic variants.

3.2. Lipidation increases the stability of the ApoA-I amyloidogenic variants

The thermal stability of LB ApoA-I variants, as well as the secondary structure rearrangements during the thermal unfolding process, were evaluated by SRCD spectroscopy (Fig. 2).

Analyses were performed by collecting the spectra in the 25–85 °C range, with a 10 °C increment. Changes in protein secondary structure (Fig. 2a–b) revealed that all ApoA-I variants, as well as the WT protein, had high thermal stability. Indeed, the decrease of the α-helical structure, with the concomitant increase of the other secondary structure elements, was found to be a gradual process, reaching a minimum at around 75–85 °C. Importantly, at the end of the denaturation process (85 °C), the decrease in the α-helical content, along with the concomitant increase in the β and unordered structures, was more extensive in the case of the amyloidogenic variants than in the WT protein. Indeed, the α-helical content dropped to around 20% in the case of the four amyloidogenic variants whereas it decreased only 34% in the native protein, where the contribution of the other secondary structure elements remained relatively low (19% β or turn, and 25% unordered in WT protein *vs* 30% β or turn, and about 25% unordered in the amyloidogenic variants). It is also worth to notice that the G26R and L75P were the most sensitive to the thermal unfolding since, in these variants, significant decrease in the α-helical content occurred at a lower temperature (45 °C for G26R and L75P *vs* 55 °C for both the other two variants and the WT protein).

Then, a complementary proteolysis approach coupled to mass spectrometry was employed to map the exposed and flexible regions in both LF and LB ApoA-I proteins, thus allowing the detection of conformational alterations in the different ApoA-I variants (Fig. 3). Complementary proteolysis experiments were carried out in strictly controlled conditions (*i.e.* E:S ratios and time of hydrolysis) and cleavage sites were determined by mass-spectroscopic identification of the generated peptides [36,37].

The results of the limited proteolysis experiments on LF proteins are shown in Fig. 3a and reported in Tables S1–S4 in Supplementary materials. All LF proteins showed a similar global accessibility and, in particular, all proteins presented several proteolytic cleavage sites at the N-terminus (region 1–57), between the residues 131–136 and at the C-terminus from residue 188 to residue 223. However, at an equal E:S ratio, all ApoA-I variants became more susceptible to proteolysis than the WT protein, as demonstrated by the higher number of cleavage sites identified. The central region spanning residues 131–153 was more accessible to proteases in the variants than in the WT protein, for which the region sensitive to the proteolysis involved residues 131–136. Specific proteolytic cleavages were also observed at positions close to the mutation sites. Indeed, in the G26R mutant digestion occurred at R27, immediately downstream the mutation spot, whereas in L174S and L178H species, additional enzymatic cleavages occurring at Y166/R173 and L159/R173, respectively, indicated the presence of local perturbation in protein conformation induced by the amino acid changes.

The proteolytic patterns of LB proteins are shown in Fig. 3b. A large reduction in the number of cleavage sites was clearly observed in all HDL-bound ApoA-I proteins compared to LF suggesting that the presence of lipids increased the overall proteins compactness and stability. The largest protective effect caused by the lipidation occurred in the central region at the C-terminus for the variants as well as for the WT ApoA-I. Specific protease accessibility was still observed for the G26R variant at R26 and R27, and for the L174S and L178H variants at R173,

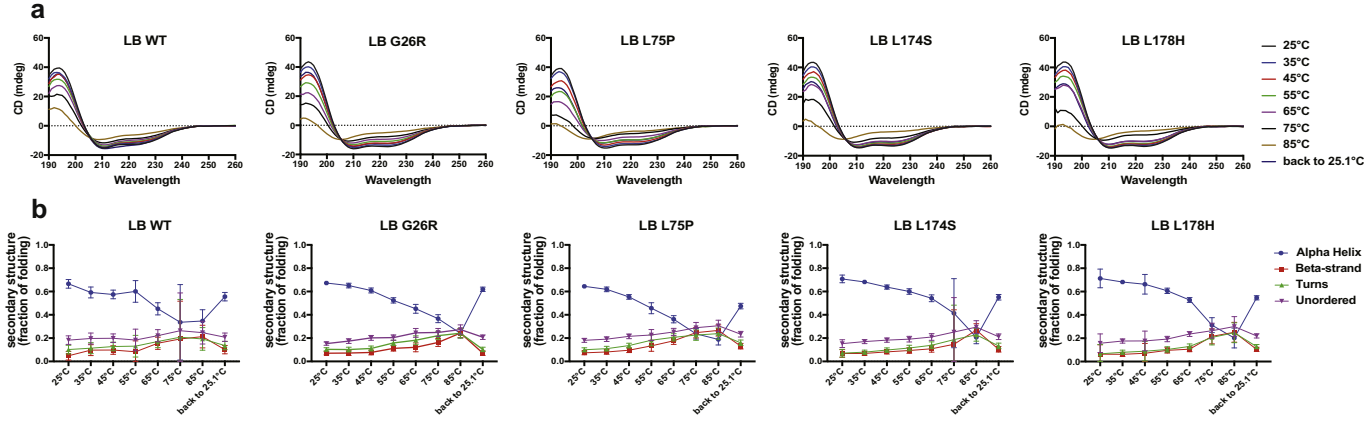

Fig. 2. Thermal stability of ApoA-I amyloidogenic variants. (a) SRCD spectra and (**b**) secondary structure estimation of LB proteins during thermal unfolding. Data shown are the mean ± SEM.

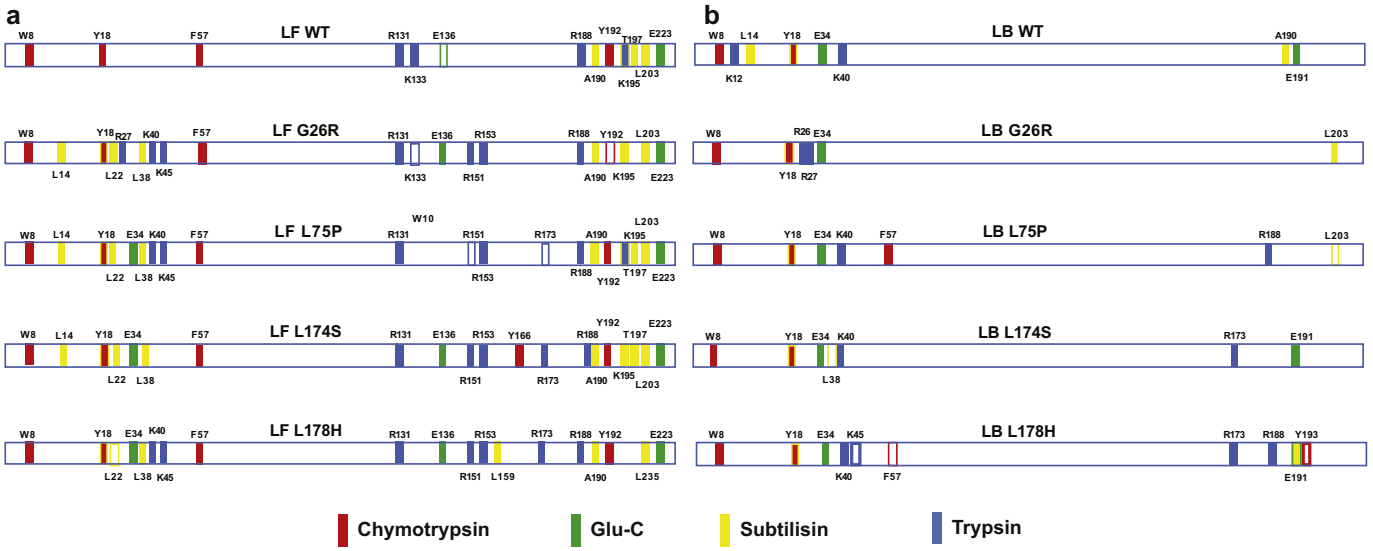

Fig. 3. Pattern of preferential proteolytic sites in WT and ApoA-I amyloidogenic variants. Schematic representation of the results obtained from complementary proteolysis experiments on LF (**a**) and LB (**b**) ApoA-I proteins. Proteolytic sites are marked as primary (filled) or secondary sites (empty) based on kinetics.

confirming a local destabilization induced by the presence of mutations. An opposite trend was observed at the N-terminus of the amyloidogenic proteins where, in general, the accessibility to this region was partially reduced compared to the LF proteins. In contrast, the N-terminus of the WT ApoA-I protein became more accessible the LB form.

3.3. The lipid binding activity is affected in the amyloidogenic ApoA-I variants

A lipid-binding assay was then performed to study the functional properties of the ApoA-I amyloidogenic variants, as ApoA-I exerts its main functional role when bound to phospholipids and cholesterol.

The lipid-binding capacity was determined by a lipid clearance assay (Fig. 4), in which the decrease of the absorbance at 325 nm due to the clearance of multilamellar DMPC vesicles by the LF proteins is measured. The rate of DMPC binding was expressed as $t_{1/2}$, calculated by fitting the experimental data with a one-way decay curve of non-linear regression (Fig. 4a). Interestingly, the kinetics of lipid binding was slower for all the amyloidogenic variants analyzed, with a 3-fold increase in the $t_{1/2}$ for G26R and L75P variants and a 7-fold and 4-fold increase for the L174S and L178H variants, respectively, compared to WT (Fig. 4b).

Then, the formation of reconstituted HDL particles was followed over time. Recombinant proteins were incubated at 24 °C with multilamellar DMPC vesicles (1:100 protein to lipid molar ratio) for the indicated length of time and analyzed by Native PAGE (Fig. 5a) and SRCD spectroscopy (Fig. 5b).

As shown in Fig. 5a, all the amyloidogenic ApoA-I variants were able to form similar intermediate structures as the WT protein, with the formation of rHDL particles of approximately 10 nm diameter already after 24 h of incubation. Although the formation of the rHDL particles was a gradual, time-dependent process, the conformational changes in the secondary structure (Fig. 5b) were found to be very fast. In particular, L178H and the WT protein underwent a significant conformational transition as soon as they were mixed with DMPC vesicles (time 0 and 0.5 in Fig. 5b), reaching a value of α-helical content very similar to that of the fully formed rHDL particles and with minor secondary structure's rearrangements during the process. The other amyloidogenic variants, instead, showed a more gradual structural rearrangement, reaching a value of helicity close to that of the final stage only upon 1 h incubation at 24 °C.

The formation of lipoparticles was also followed in a more physiological environment. For this purpose, proteins were incubated in mouse serum at 37 °C (Fig. 6).

The formation of recombinant HDL was monitored over time by western blot analysis using antibodies directed towards human ApoA-I. The incubation of ApoA-I in mouse serum appeared to lead to the incorporation of the human protein in existing mouse HDL particles, as antibodies directed towards either human or mouse ApoA-I coincided in western blot analyses (data not shown). WT-ApoA-I was able to efficiently form HDL already after 0.5 h of incubation, with no apparent immuno-signal associated with LF protein after 2 h of incubation.

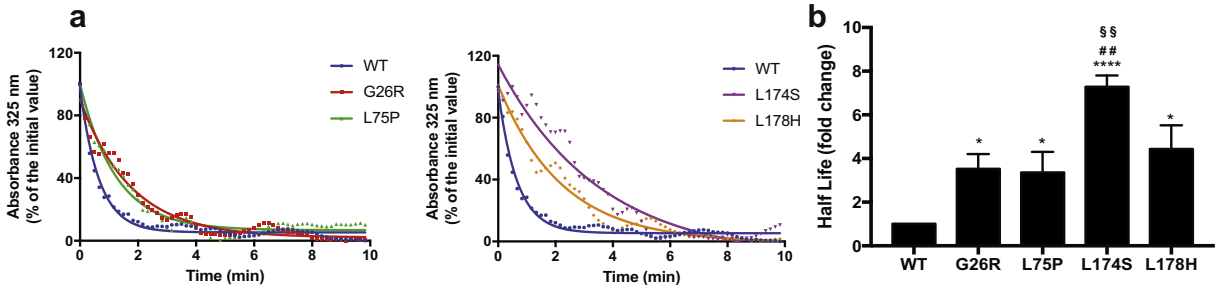

Fig. 4. ApoA-I amyloidogenic variants have a decreased lipid binding efficiency. (**a**) Lipid Clearance Assay. Proteins were incubated with multilamellar DMPC vesicles with a 1:100 lipid to protein molar ratio and the decrease of the absorbance at 325 nm was measured every 10 s for 10 min. Experimental points were fitted to one-way decay of non-linear regression and the rates of lipid binding were calculated (**b**). Data shown are the mean ± SEM of 5 independent experiments carried out in triplicate. Significance is calculated according to one-way ANOVA ($^{*}p < 0.05$, $^{***}p < 0.001$ for groups as shown with respect to the WT protein, $^{\#\#}p < 0.01$ for groups as shown with respect to G26R variant, $^{\S\S}p < 0.01$ for groups as shown with respect to L75P variant).

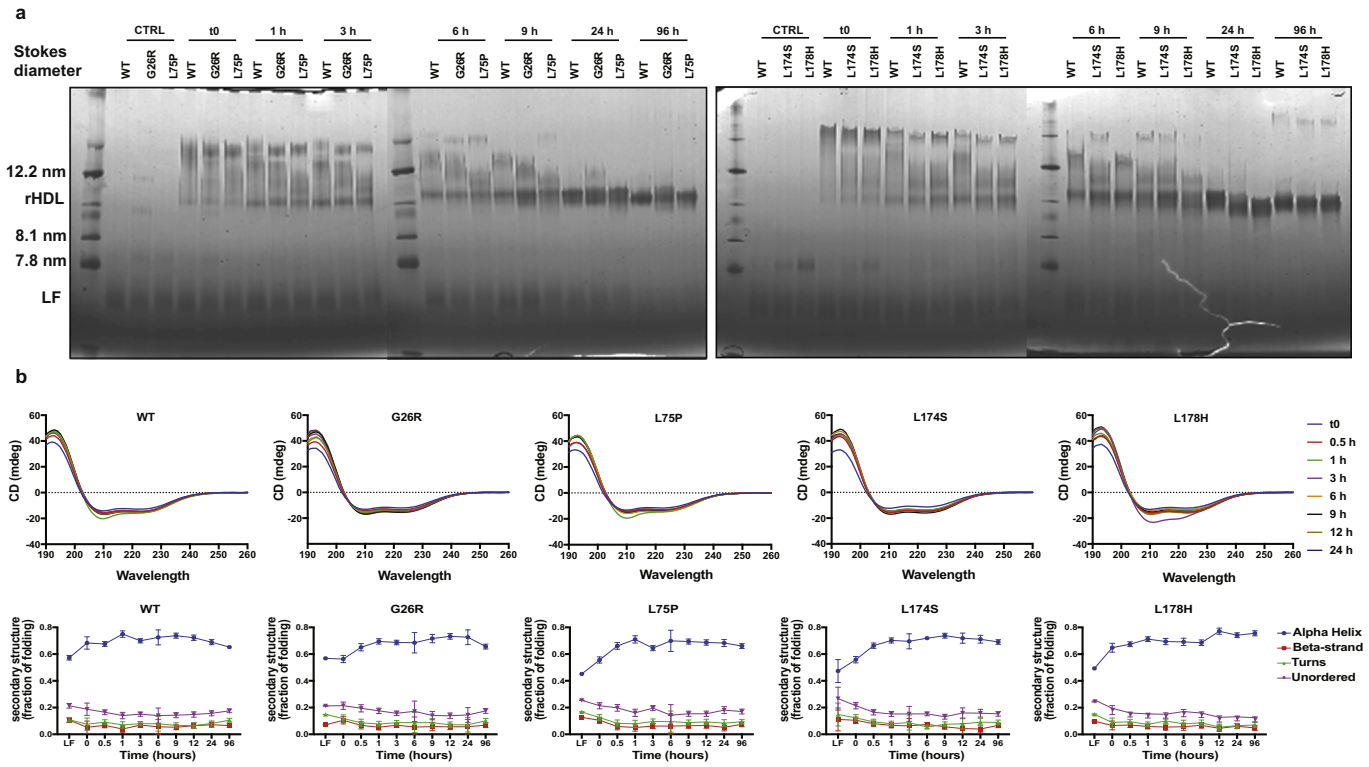

Fig. 5. ApoA-I amyloidogenic variants' ability to form rHDL*s in vitro*. Proteins were incubated with DMPC vesicles (1:100 lipid to protein molar ratio) at 24 °C for the indicated times. (**a**) Blue Native Page analysis of rHDL formation. Lipid free (LF) proteins were loaded as controls. (**b**) Protein secondary structure analysis during the rHDL formation.

Interestingly, all the amyloidogenic variants showed a reduced efficiency to form HDL in mouse serum with LF protein observed also after 24 h of incubation.

The decreased affinity of the amyloidogenic variants for the lipids in this physiological-like environment, along with an enhanced metabolism of the lipid free protein, may explain the lower serum levels of the ApoA-I proteins (both variant and the WT) found in patients affected by ApoA-I related amyloidosis [19–23].

3.4. ApoA-I amyloidogenic variants have improved efficiency at catalysing cholesterol efflux

As the main function of lipidated ApoA-I is to efflux cholesterol from macrophages at the vascular wall that is redirected to the liver where it is catabolized, we next analyzed the ability of ApoA-I amyloidogenic variants to catalyze cholesterol efflux from J774 macrophages.

Macrophages were loaded with ^{3}H-cholesterol, pre-incubated with Cpt-cAMP to induce the expression of ABCA1 and incubated with either lipid free (LF) or lipid bound (LB) proteins as acceptors of cholesterol, in concentration- and time-dependent experiments. As shown in Fig. 7, although the amyloidogenic variants (both LF or LB states) seemed to have a lower efflux capacity (low B_{max}, Fig. 7e and f), they were found to have a higher efficiency (low K_d) to efflux cholesterol compared to the WT protein (Fig. 7c and d). In particular, the L174S and L178H variants showed the highest efficiency with a decrease in the K_d of 79% and 64% at 4 h, in their LF state (Fig. 7c, right panel), and of 42% and 33% at 4 h and 60% and 55% at 24 h in their LB state (Fig. 7d, middle and right panel) compared to WT (in LF and LB states, respectively). Also, in the LF state, the L75P variant displayed a higher efflux efficiency at 4 h of efflux compared to WT protein (40% decrease in the K_d for LF L75P compared to the native LF protein), while in the LB state, the L75P showed a higher efficiency (64% decrease in K_d, compared to the WT) only in the 24 h efflux (Fig. 7d, right panel). Finally, although the G26R variant was not significantly different from the WT protein in

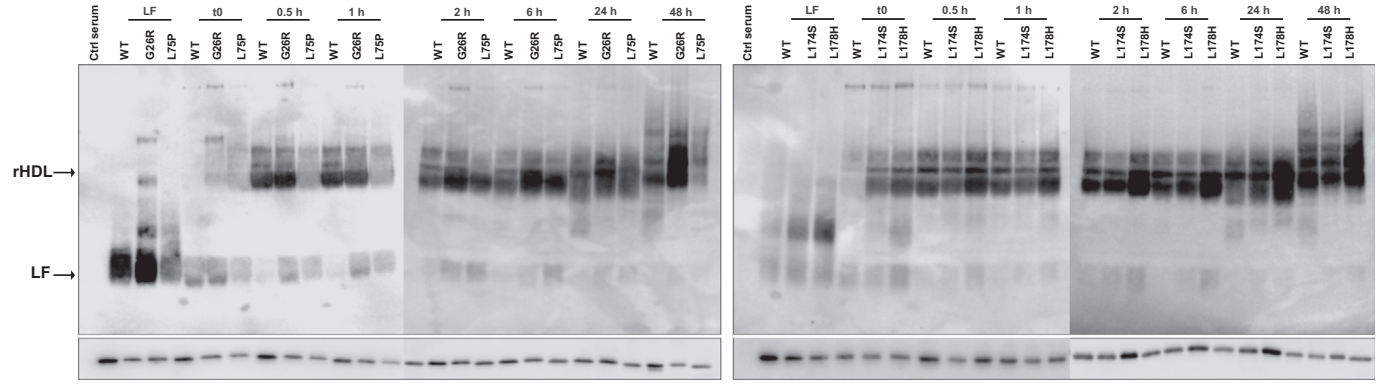

Fig. 6. ApoA-I variants have a lower efficiency at forming rHDL in mouse serum. ApoA-I amyloidogenic variants were incubated with mouse serum at 37 °C for the indicated times. Samples were separated by native (**upper panels**) and denaturant (**lower panels**) electrophoresis and analyzed by Western Blotting using specific antibodies towards human ApoA-I. LF proteins and mouse serum (ctrl serum) were loaded as controls. Arrows indicate the LF proteins and rHDL particles with a diameter of about 10 nm.

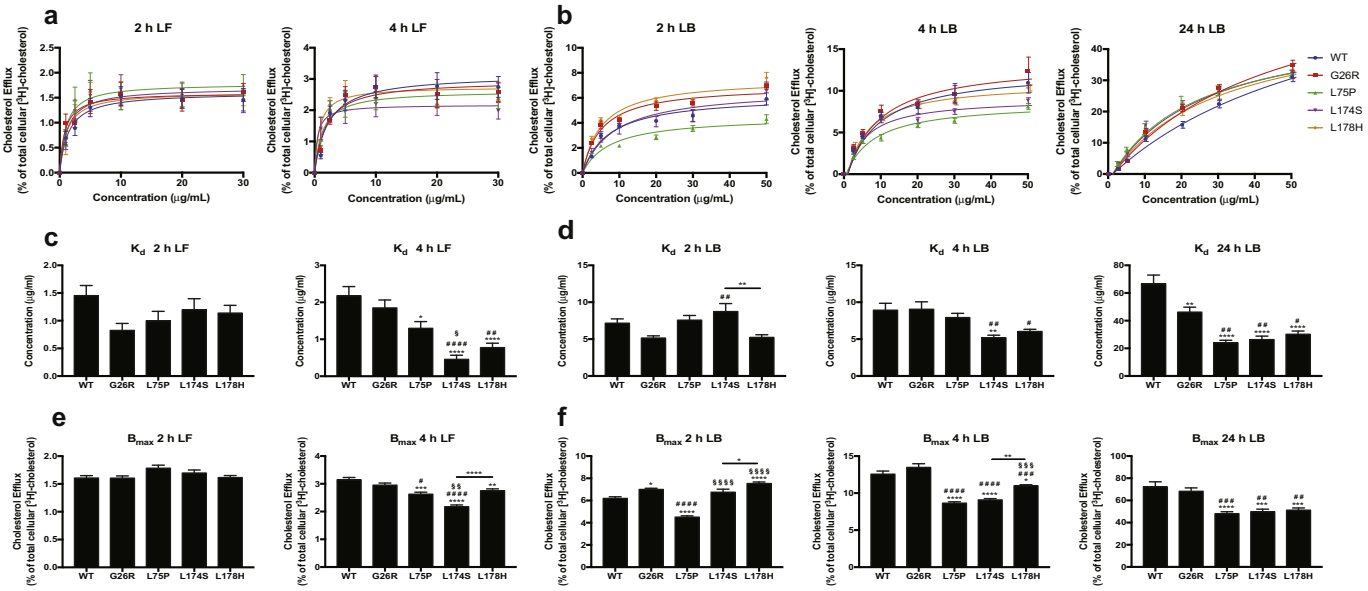

Fig. 7. Effect of amyloidogenic mutations on the cholesterol efflux by Apo A-I variants. J774 macrophages enriched with ^{3}H-cholesterol were incubated with LF (**a**, **c**, **e**) or LB (**b**, **d**, **f**) amyloidogenic variants for 2, 4 and 24 h, at the indicated protein concentration. An ACAT inhibitor and CPT-cAMP were used to prevent the formation of cholesteryl esters of ^{3}H-cholesterol and to induce the expression of ABCA1, respectively. The ^{3}H-cholesterol efflux in the treatment media was quantified as a function of concentration (**a**, **b**). The experimental data were fitted (**a**, **b**) and K_d and B_{max} were calculated according to the Michaelis-Menten equation (**c**, **d**, **e**, **f**). Data shown are the mean ± SEM (n = 9 and 6 for LF and LB, respectively). Significance is calculated according to one-way ANOVA ($^{*}p < 0.05$, $^{**}p < 0.005$, $^{***}p < 0.001$, $^{****}p < 0.0001$ for groups as shown with respect to the WT protein, $^{\#}p < 0.05$, $^{\#\#}p < 0.005$, $^{\#\#\#}p < 0.001$, $^{\#\#\#\#}p < 0.0001$ for groups as shown with respect to G26R variant, $^{\S}p < 0.05$, $^{\S\S}p < 0.005$, $^{\S\S\S}p < 0.001$, $^{\S\S\S\S}p < 0.0001$ for groups as shown with respect to L75P variant).

their LF state, it showed a significant higher affinity in the efflux analyses (31% decrease in the K_d compared to WT) when lipid bound (Fig. 7d, right panel). It is also worth to notice that the L174S and L178H variants were more efficient in catalysing cholesterol efflux from macrophages compared to the other variants, especially when the efflux was carried out for 4 h.

The DMPC (14:0) lipids provide the important advantage that formation of the protein-lipid complexes can be assayed in real-time at physiological-like buffer conditions without the need for solubilizing detergents. However, lipids such as POPC (16:0) better mimics mammalian phospholipid compositions thus better resembling the physiological HDL particles. The efflux capacity of ApoA-I amyloidogenic variants in complex with POPC was therefore analyzed.

POPC-ApoA-I particles were produced by incubating the recombinant proteins with POPC at a 1:80 protein to lipid ratio and a protein concentration of 0.5 mg/ml. The formed POPC rHDLs were then analyzed by native gel electrophoresis (Fig. 8a) and, as in the case of DMPC-bound proteins, the particles formed by the L174S and L178H variants were smaller with respect to those containing the WT protein, G26R and L75P variants, confirming that the position of the mutation in the ApoA-I sequence contribute to unique structures of the formed rHDLs.

POPC-ApoA-I HDL were tested for their ability to remove cholesterol from J774 macrophages (Fig. 8b). As already observed for DMPC-ApoA-I rHDL, POPC-ApoA-I particles formed by the amyloidogenic variants were all found to be more efficient at catalysing cholesterol efflux, at both time points analyzed. L174S and L178H showed the highest efficiency (Fig. 8c) with a K_d reduction of 79% and 82% at 2 h and 79% and 76% at 4 h, compared to the POPC particles formed by the WT protein. However, differently from what observed in the case of DMPC bound proteins, also the POPC particles formed by G26R and L75P variants were characterized by a very high efficiency in removing cholesterol from macrophages, showing a K_d reduction of 68% and 58% at 2 h and 59% and 64% at 4 h, compared to the POPC-ApoA-I particles formed by the native protein.

4. Discussion

The hallmark of ApoA-I hereditary systemic amyloidosis is the progressive accumulation of protein fibrils in the extracellular space of target tissues, a mechanism that leads to organ dysfunction and failure [2–4]. In addition, subjects affected by this pathology show low plasma levels of both the native and the amyloidogenic variant and a peculiar lipid profile, characterized by low levels of HDL and HDL-cholesterol [18–22]. Nevertheless, despite this unfavourable lipid profile, carriers of ApoA-I amyloidogenic mutations do not show an increased risk of CVD, suggesting that a compensative, protective mechanism may exist [22]. To explore the structural and functional features of ApoA-I amyloidogenic variants responsible for the clinical phenotype, we chose four ApoA-I amyloidogenic variants representative of the two 3D hot-spot mutation sites defined in the X-ray structure of the C-terminal truncated version of protein [27], with the G26R and L75P being located in the N-terminal hot spot region (residues 26–107) and the L174S and L178H in the hot spot region encompassing residues 154–178 [28].

We clearly demonstrate, as previously reported only for the WT protein [38,39], that lipidation stabilizes and protects the amyloidogenic variants from proteolysis. Indeed, the complementary proteolysis experiments on LB proteins (Fig. 3b) showed a large reduction in the number of cleavage sites compared to LF samples (Fig. 3a), suggesting that the presence of lipids largely increases ApoA-I variants proteins stability. This findings are also supported by the higher E:S ratios used for the LB proteins in comparison with the respective LF forms. We also demonstrate that the presence of an amyloidogenic mutation in ApoA-I sequence represents a risk factor able to shift the equilibrium from a lipid-bound towards a lipid-free conformation. Indeed, although all the ApoA-I amyloidogenic variants were able to produce rHDL particles both *in vitro* (Figs. 4, 5) and *ex vivo* (Fig. 6), they showed a significant decreased affinity for lipids, with L174S and L178H with the lowest lipid binding affinity. Moreover, proteolytic cleavages were still observed close to the mutation site (R26 and R27 in G26R, R173 in L174S and L178H), confirming that the presence of the mutation alters the

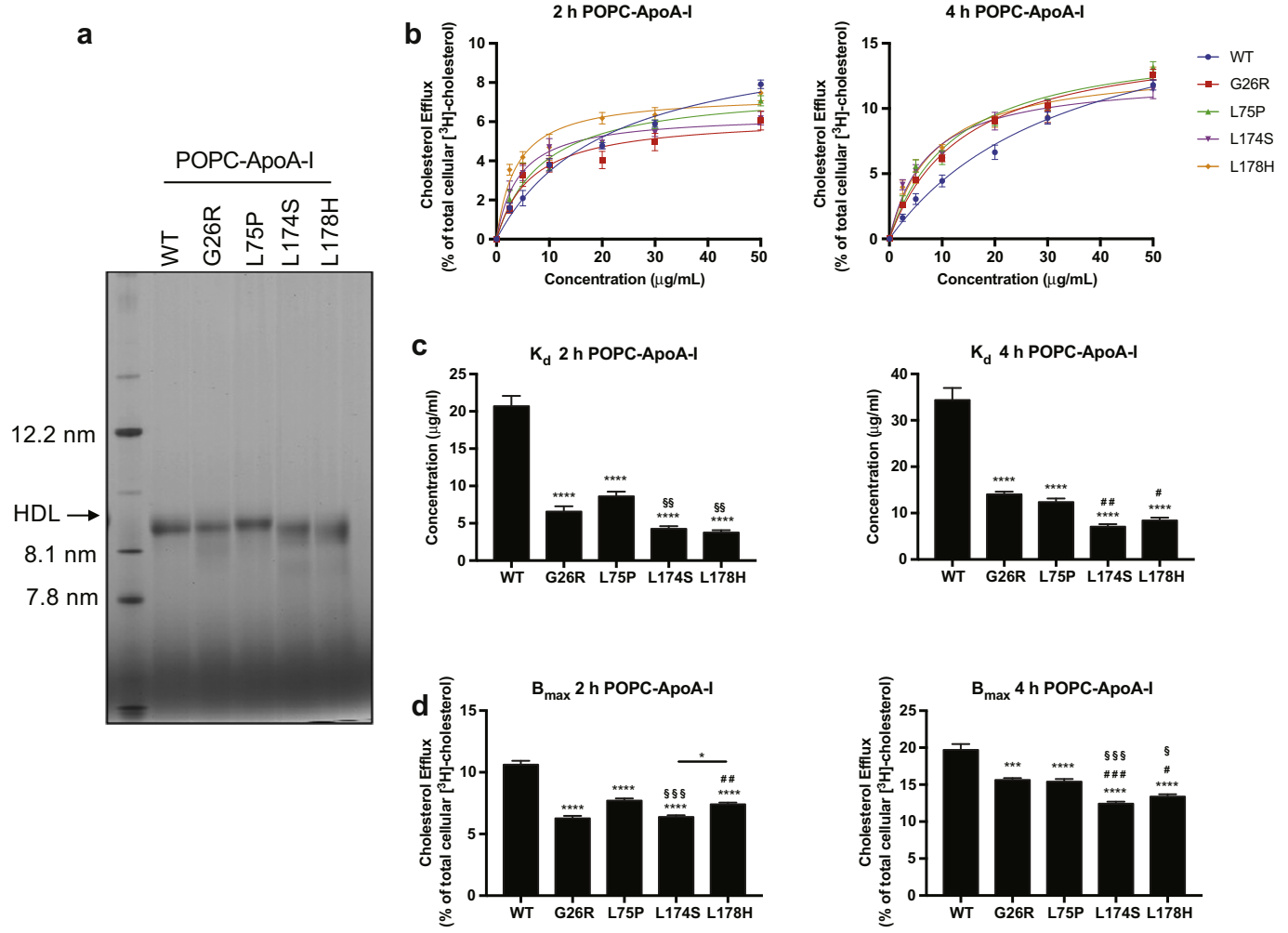

Fig. 8. Cholesterol efflux ability of POPC-ApoA-I variants. ApoA-I amyloidogenic variants were incubated with POPC (1:80 protein to lipids molar ratio) and lipoparticles formed by the cholate dialysis method. POPC-ApoA-I HDL were analyzed by Blue Native PAGE (**a**). J774 macrophages enriched with ^{3}H-cholesterol were incubated with the POPC-ApoA-I particles for 2 h and 4 h and the ^{3}H-cholesterol efflux in the treatment media was quantified as a function of protein concentration (**b**). The fitting of the experimental data allowed the calculation of K_d and B_{max} (**c**, **d**). Data shown are the mean ± SEM ($n = 6$). Significance is calculated according to one-way ANOVA ($^{*}p < 0.05$, $^{***}p < 0.001$, $^{****}p < 0.0001$ for groups as shown with respect to the WT protein, $^{\#}p < 0.05$, $^{\#\#}p < 0.005$, $^{\#\#\#}p < 0.001$, for groups as shown with respect to G26R variant, $^{\S}p < 0.05$, $^{\S\S}p < 0.005$, $^{\S\S\S}p < 0.001$, for groups as shown with respect to L75P variant).

local conformation of the protein. Consistent with our results, by using a hydrogen-deuterium exchange approach, Das and co-workers found that L170P and L159R ApoA-I variants were characterized by a high solvent accessibility and caused the largest lipoprotein destabilization, compared to W50R, G26R and F71Y variants [17].

The DLS and native gel analyses on rHDL (Fig. 1b) showed that the lipoparticle formed by the L174S and L178H variants had a smaller size with respect to those produced by G26R and L75P variants and SRCD analyses revealed that L174S- and L178H-rHDLs were characterized by a higher α-helical content (Fig. 1d, right panel). The difference observed between the two classes of variants are not surprising if we consider that the C-terminal domain of ApoA-I is characterized by the highest hydrophobicity and it is known to mediate the binding to lipids and to initiate the formation of HDLs [40,41]. Therefore, the presence of mutations in close proximity to the protein C-terminus could destabilize this domain and alter its interaction with lipids, conferring to the variants a lower ability to form lipoparticles.

The analysis of the ApoA-I proteins in their LF form also revealed interesting differences among the variants and the native protein. SRCD data obtained at increasing protein concentrations (Fig. 1c and d) indicate that, although the conformation and oligomeric state of the variants are dependent on protein concentration, as demonstrated for the native protein [42], the degree of structural rearrangements could be influenced by the position of the mutation in the protein sequence. Indeed, the C-terminal domain of ApoA-I is known to participate in the self-association of the protein, as demonstrated by the inability of the deletion mutants 185–243 and 209–243 to form oligomers in solution [43]. The EPR analyses conducted on the native protein also supported this hypothesis, identifying the C-terminal domain as the most sensitive to molecular crowding [42]. Thus, the destabilization of the C-terminal imposed by the presence of mutations might be responsible for the impeded conformational change observed in the variants.

LF ApoA-I amyloidogenic variants also showed a higher susceptibility to proteolysis compared to the native protein, in agreement with our previous reports [13,14,17]. The higher susceptibility of all ApoA-I variants in the region close to the mutation sites suggested an increase of local flexibility and exposure to solvent and indicates that all single point mutations result in a large destabilization of the four-helix bundle motif [28,44]. In addition to proteolytic cleavages close to the mutation site, all the variants were characterized by an enhanced susceptibility in both N- and C-termini and in the region encompassing residues 131–153. Notably, all these regions have also been described to have a role in the HDL formation. In particular, Pollard and co-workers have recently confirmed that the N- and C-terminal domain of ApoA-I participate in the process of lipidation and their destabilization slow down the rHDL formation and demonstrated that the flexibility and the

opening of the central region of the protein is essential for the formation of the discoidal rHDLs [45].

Taken together, our results suggest that the decreased lipid affinity and the enhanced proteolytic susceptibility that characterize ApoA-I amyloidogenic variants may explain the low ApoA-I and HDL plasma levels observed in affected carriers. Nevertheless, these observations are in contrast with the cardiovascular state of ApoA-I amyloidogenic carriers, since the significant reduction of ApoA-I and HDL levels should imply a higher CVD risk. Our data on the ability of the ApoA-I amyloidogenic variants to efflux cholesterol from macrophages contribute to explain this paradox. Indeed, all the ApoA-I variants, especially in their LB state (either DMPC- or POPC-bound), showed a higher efficiency in catalysing the removal of cholesterol from macrophages (Figs. 7 and 8). Surprisingly, the variants showing the lowest lipid binding affinity, L174S and L178H, were found to have the highest efficiency in this process. We therefore hypothesize that the altered conformations acquired by the mutated proteins stabilize the interaction of the rHDL with ABCA1, thus enhancing the efflux of cholesterol from macrophages. Another factor able to stabilize this interaction could be represented by the amino acid substitution itself. This is also suggested by studies on lipoparticles formation with ApoA-I cysteine mutants in the presence of ABCA1-expressing HEK293 cells [45], where the substitution of charged amino acids with cysteines dramatically reduced the amount of HDL particles formation. In the same way, the substitution of a hydrophobic amino acid with a polar or charged amino acid, as in the case of L174S and L178H, could stabilize the binding between the ApoA-I variant in the rHDL and ABCA1 on macrophages cell surface.

The structural features here described for the amyloidogenic variants are in line with previous reports on the R173C variant, also known as Milano, an ApoA-I non-amyloidogenic variant [46] associated with a decreased risk of CVD [47]. Indeed, in a structural and functional study, Alexander and co-workers demonstrated that ApoA-I Milano was characterized by a lower stability, lower affinity for lipids and it was able to give rise to HDL with a slightly smaller size [48]. Nevertheless, Milano variant did not show any improved ability to efflux cholesterol from macrophages suggesting that, in this case, the atheroprotection observed in carriers of R173C is due to other factors than increased cholesterol mobilization [49].

Although our studies show a connection between ApoA-I variants' structural features and their ability to bind cholesterol, further experiments will be carried out by using HDL particles isolated from patients carrying these mutations in order to give strength to our findings and to validate their biological relevance. In addition, while the SRCD and limited proteolysis data provide important knowledge about protein secondary structure, accessibility and stability, high-resolution 3D structures of ApoA-I variants in nascent HDL are lacking. The determination of such protein-lipid complexes is very challenging but could potentially be resolved by using cryo-electron microscopy [50], electron paramagnetic resonance spectroscopy [51] and/or X-ray crystallography [27], thus giving new insights in the structure to function properties of ApoA-I amyloidogenic variants.

5. Conclusions

The study shows that the position in the ApoA-I sequence of an amyloidogenic mutation differently affects both the protein affinity for lipids and the molecular structure of the formed HDL. Interestingly, the amyloidogenic variants' reduced capability in forming HDL particles is well compensated with a higher efficiency at catalysing cholesterol efflux from macrophages. Our findings define the ApoA-I variants' higher efficiency in the cholesterol efflux process as a protective mechanism able to compensate the unfavourable lipid profile of patients affected by ApoA-I related amyloidosis, allowing us to provide explanation to the paradox observed in the clinical phenotype.

Supplementary data to this article can be found online at http://dx.doi.org/10.1016/j.bbadis.2017.09.001.

Author's contributions

RDG designed the study, researched and evaluated data and wrote the first draft of the manuscript; JDE, II and ON researched and evaluated data; MM and DMM evaluated data and contributed to the writing of the manuscript; JOL designed the study, evaluated data and contributed to the writing of the manuscript. All authors approved the final version of the manuscript.

Transparency document

The Transparency document associated with this article can be found, in online version.

Acknowledgments

The authors thank Miss Hughes, C. and, Drs Hussain, R., and Siligardi, G. at Diamond Light Source beamline B23 (project number SM14703-2) for valuable support in the SRCD analyses. This work was supported by grants from the Swedish Research Council (K2014-54X-22426-01-3), the Royal Physiographic Society in Lund, and the Blanceflor foundation.

References

[1] M.D. Benson, Ostertag revisited: the inherited systemic amyloidoses without neuropathy, Amyloid 12 (2005) 75–87.
[2] L. Obici, G. Franceschini, L. Calabresi, S. Giorgetti, M. Stoppini, G. Merlini, V. Bellotti, Structure, function and amyloidogenic propensity of apolipoprotein A-I, Amyloid 13 (2006) 1–15.
[3] D. Rowczenio, A. Dogan, J.D. Theis, J.A. Vrana, H.J. Lachmann, A.D. Wechalekar, J.A. Gilbertson, T. Hunt, S.D. Gibbs, P.T. Sattianayagam, et al., Amyloidogenicity and clinical phenotype associated with five novel mutations in apolipoprotein A-I, Am. J. Pathol. 179 (2011) 1978–1987.
[4] M. Gomaraschi, L. Obici, S. Simonelli, G. Gregorini, A. Negrinelli, G. Merlini, G. Franceschini, L. Calabresi, Effect of the amyloidogenic L75P apolipoprotein A-I variant on HDL subpopulations, Clin. Chim. Acta 412 (2011) 1262–1265.
[5] K.A. Rye, P.J. Barter, Formation and metabolism of prebeta-migrating, lipid-poor apolipoprotein A-I, Arterioscler. Thromb. Vasc. Biol. 24 (2004) 421–428.
[6] V.I. Zannis, A. Chroni, M. Krieger, Role of apoA-I, ABCA1, LCAT, and SR-BI in the biogenesis of HDL, J. Mol. Med. 84 (2006) 276–294.
[7] Emerging Risk Factors Collaboration, E. Di Angelantonio, N. Sarwar, P. Perry, S. Kaptoge, K.K. Ray, A. Thompson, A.M. Wood, S. Lewington, N. Sattar, C.J. Packard, R. Collins, S.G. Thompson, J. Danesh, Major lipids, apolipoproteins, and risk of vascular disease, JAMA 302 (2009) 1993–2000.
[8] L. Pastore, L.M. Belalcazar, K. Oka, R. Cela, B. Lee, L. Chan, A.L. Beaudet, Helper-dependent adenoviral vector-mediated long-term expression of human apolipoprotein AI reduces atherosclerosis in apo E-deficient mice, Gene 327 (2004) 153–160.
[9] C.G. Brouillette, G.M. Anantharamaiah, J.A. Engler, D.W. Borhani, Structural models of human apolipoprotein AI: a critical analysis and review, Biochim. Biophys. Acta 1531 (2001) 4–46.
[10] K.A. Rye, M.A. Clay, P.J. Barter, Remodelling of high density lipoproteins by plasma factors, Atherosclerosis 145 (1999) 227–238.
[11] M. Eriksson, S. Schonland, S. Yumlu, U. Hegenbart, H. von Hutten, Z. Gioeva, P. Lohse, J. Büttner, H. Schmidt, C. Röcken, Hereditary apolipoprotein AI-associated amyloidosis in surgical pathology specimens: identification of three novel mutations in the APOA1 gene, J. Mol. Diagn. 11 (2009) 257–262.
[12] F.W. Vonberg, J.A. Gilbertson, D. Rowczenio, D.F. Hutt, N. Rendell, G. Taylor, P.N. Hawkins, J.D. Gillmore, Amyloid cardiomyopathy associated with a novel apolipoprotein A–I Q172P variant, Amyloid 22 (2015) 252–253.
[13] J.O. Lagerstedt, G. Cavigiolio, L.M. Roberts, H.S. Hong, L.W. Jin, P.G. Fitzgerald, M.N. Oda, J.C. Voss, Mapping the structural transition in an amyloidogenic apolipoprotein A-I, Biochemistry 46 (2007) 9693–9699.
[14] J. Petrlova, T. Duong, M.C. Cochran, A. Axelsson, M. Mörgelin, L.M. Roberts, J.O. Lagerstedt, The fibrillogenic L178H variant of apolipoprotein A-I forms helical fibrils, J. Lipid Res. 53 (2012) 390–398.
[15] M. Das, X. Mei, S. Jayaraman, D. Atkinson, O. Gursky, Amyloidogenic mutations in human apolipoprotein A-I are not necessarily destabilizing—a common mechanism of apolipoprotein A-I misfolding in familial amyloidosis and atherosclerosis, FEBS J. 281 (2014) 2525–2542.
[16] S.A. Rosú, O.J. Rimoldi, E.D. Prieto, L.M. Curto, J.M. Delfino, N.A. Ramella, M.A. Tricerri, Amyloidogenic propensity of a natural variant of human apolipoprotein a-I: stability and interaction with ligands, PLoS One 10 (2015) e0124946.
[17] R. Del Giudice, A. Arciello, F. Itri, A. Merlino, M. Monti, M. Buonanno, A. Penco,

D. Canetti, G. Petruk, S.M. Monti, A. Relini, P. Pucci, R. Piccoli, D.M. Monti, Protein conformational perturbations in hereditary amyloidosis: differential impact of single point mutations in ApoAI amyloidogenic variants, Biochim. Biophys. Acta 1860 (2016) 434–444.
[18] M. Das, C.J. Wilson, X. Mei, T.E. Wales, J.R. Engen, O. Gursky, Structural stability and local dynamics in disease-causing mutants of human apolipoprotein A-I: what makes the protein amyloidogenic? J. Mol. Biol. 428 (2016) 449–462.
[19] D.J. Rader, R.E. Gregg, M.S. Meng, J.R. Schaefer, L.A. Zech, M.D. Benson, H.B. Jr Brewer, In vivo metabolism of a mutant apolipoprotein, apoA-IIowa, associated with hypoalphalipoproteinemia and hereditary systemic amyloidosis, J. Lipid Res. 33 (1992) 755–763.
[20] G. Gregorini, C. Izzi, P. Ravani, L. Obici, N. Dallera, A. Del Barba, A. Negrinelli, R. Tardanico, M. Nardi, L. Biasi, T. Scalvini, G. Merlini, F. Scolari, Tubulointerstitial nephritis is a dominant feature of hereditary apolipoprotein A-I amyloidosis, Kidney Int. 87 (2015) 1223–1229.
[21] L. Obici, V. Bellotti, P. Mangione, M. Stoppini, E. Arbustini, L. Verga, I. Zorzoli, E. Anesi, G. Zanotti, C. Campana, M. Viganò, G. Merlini, The new apolipoprotein A-I variant leu(174) → Ser causes hereditary cardiac amyloidosis, and the amyloid fibrils are constituted by the 93-residue *N*-terminal polypeptide, Am. J. Pathol. 155 (1999) 695–702.
[22] M.L. Muiesan, M. Salvetti, A. Paini, C. Agabiti Rosei, G. Rubagotti, A. Negrinelli, G. Gregorini, G. Cancarini, L. Calabresi, G. Franceschini, L. Obici, S. Perlini, G. Merlini, E. Agabiti Rosei, Vascular alteration in apolipoprotein A-I amyloidosis (Leu75Pro). A case-control study, Amyloid 22 (2015) 187–193.
[23] L. Obici, G. Palladini, S. Giorgetti, V. Bellotti, G. Gregorini, E. Arbustini, L. Verga, S. Marciano, S. Donadei, V. Perfetti, et al., Liver biopsy discloses a new apolipoprotein A-I hereditary amyloidosis in several unrelated Italian families, Gastroenterology 126 (2004) 1416–1422.
[24] W.C. Nichols, R.E. Gregg, H.B. Jr Brewer, M.D. Benson, A mutation in apolipoprotein A-I in the Iowa type of familial amyloidotic polyneuropathy, Genomics 8 (1990) 318–323.
[25] P. Mangione, M. Sunde, S. Giorgetti, M. Stoppini, G. Esposito, L. Gianelli, L. Obici, L. Asti, A. Andreola, P. Viglino, et al., Amyloid fibrils derived from the apolipoprotein A1 Leu174Ser variant contain elements of ordered helical structure, Protein Sci. 10 (2001) 187–199.
[26] M.M. de Sousa, C. Vital, D. Ostler, R. Fernandes, J. Pouget-Abadie, D. Carles, M.J. Saraiva, Apolipoprotein AI and transthyretin as components of amyloid fibrils in a kindred with apoAI Leu178His amyloidosis, Am. J. Pathol. 156 (2000) 1911–1917.
[27] X. Mei, D. Atkinson, Crystal structure of C-terminal truncated apolipoprotein A-I reveals the assembly of HDL by dimerization, J. Biol. Chem. 286 (2011) 38570–38582.
[28] O. Gursky, X. Mei, D. Atkinson, The crystal structure of the C-terminal truncated apolipoprotein A-I sheds new light on amyloid formation by the N-terminal fragment, Biochemistry 51 (2012) 10–18.
[29] J. Dalla-Riva, J.O. Lagerstedt, J. Petrlova, Structural and functional analysis of the apolipoprotein A-I A164S variant, PLoS One 10 (2015) e0143915.
[30] T. Javorfi, R. Hussain, D. Myatt, G. Siligardi, Measuring circular dichroism in a capillary cell using the B23 synchrotron radiation CD beamline at diamond light source, Chirality 22 (2010) E149–E153.
[31] R. Hussain, T. Jávorfi, G. Siligardi, Circular dichroism beamline B23 at the diamond light source, J. Synchrotron Radiat. 19 (2012) 132–135.
[32] R. Hussain, K. Benning, T. Javorfi, E. Longo, T.R. Rudd, B. Pulford, G. Siligardi, CDApps: integrated software for experimental planning and data processing at beamline B23, diamond light source, J. Synchrotron Radiat. 22 (2015) 465–468.
[33] S.W. Provencher, J. Glockner, Estimation of globular protein secondary structure from circular dichroism, Biochemistry 20 (1981) 33–37.
[34] P.G. Yancey, M.A. Kawashiri, R. Moore, J.M. Glick, D.L. Williams, M.A. Connelly, D.J. Rader, G.H. Rothblat, In vivo modulation of HDL phospholipid has opposing effects on SR-BI- and ABCA1-mediated cholesterol efflux, J. Lipid Res. 45 (2004) 337–346.
[35] S. Sankaranarayana, G. Kellner-Weibel, M. de la Llera-Moya, M.C. Phillips, B.F. Asztalos, R. Bittman, G.H. Rothblat, A sensitive assay for ABCA1-mediated cholesterol efflux using BODIPY-cholesterol, J. Lipid Res. 52 (2011) 2332–2340.
[36] A. Scaloni, M. Monti, R. Acquaviva, G. Tell, G. Damante, S. Formisano, P. Pucci, Topology of the thyroid transcription factor 1 homeodomain-DNA complex, Biochemistry 38 (1999) 64–72.
[37] G. Esposito, R. Michelutti, G. Verdone, P. Viglino, H. Hernández, C.V. Robinson, A. Amoresano, F. Dal Piaz, M. Monti, P. Pucci, P. Mangione, M. Stoppini, G. Merlini, G. Ferri, V. Bellotti, Removal of the N-terminal hexapeptide from human beta2-microglobulin facilitates protein aggregation and fibril formation, Protein Sci. 9 (2000) 831–845.
[38] O. Gursky, D. Atkinson, Thermal unfolding of human high-density apolipoprotein A-1: implications for a lipid-free molten globular state, Proc. Natl. Acad. Sci. U. S. A. 93 (1996) 2991–2995.
[39] W. Safi, J.N. Maiorano, W.S. Davidson, A proteolytic method for distinguishing between lipid-free and lipid-bound apolipoprotein A-I, J. Lipid Res. 42 (2001) 864–872.
[40] W. Huang, J. Sasaki, A. Matsunaga, H. Han, W. Li, T. Koga, M. Kugi, S. Ando, K. Arakawa, A single amino acid deletion in the carboxy terminal of apolipoprotein A-I impairs lipid binding and cellular interaction, Arterioscler. Thromb. Vasc. Biol. 20 (2000) 210–216.
[41] K. Nagao, M. Hata, K. Tanaka, Y. Takechi, D. Nguyen, P. Dhanasekaran, S. Lund-Katz, M.C. Phillips, H. Saito, The roles of C-terminal helices of human apolipoprotein A-I in formation of high-density lipoprotein particles, Biochim. Biophys. Acta Mol. Cell Biol. Lipids 2014 (1841) 80–88.
[42] J. Petrlova, S. Hilt, M. Budamagunta, J. Domingo-Espin, J.C. Voss, J.O. Lagerstedt, Molecular crowding impacts the structure of apolipoprotein A-I with potential implications on in vivo metabolism and function, Biopolymers 105 (2016) 683–692.
[43] M. Laccotripe, S.C. Makrides, A. Jonas, V.I. Zannis, The carboxyl-terminal hydrophobic residues of apolipoprotein A-I affect its rate of phospholipid binding and its association with high density lipoprotein, J. Biol. Chem. 272 (1997) 17511–17522.
[44] A. Arciello, R. Piccoli, D.M. Monti, Apolipoprotein A-I: the dual face of a protein, FEBS Lett. 590 (2016) 4171–4179.
[45] R.D. Pollard, B. Fulp, M.G. Sorci-Thomas, M.J. Thomas, High-density lipoprotein biogenesis: defining the domains involved in human apolipoprotein A-I lipidation, Biochemistry 55 (2016) 4971–4981.
[46] J. Petrlova, J. Dalla-Riva, M. Mörgelin, M. Lindahl, E. Krupinska, K.G. Stenkula, J.C. Voss, J.O. Lagerstedt, Secondary structure changes in ApoA-I Milano (R173C) are not accompanied by a decrease in protein stability or solubility, PLoS One 9 (2014) e96150.
[47] C.R. Sirtori, L. Calabresi, G. Franceschini, D. Baldassarre, M. Amato, J. Johansson, M. Salvetti, C. Monteduro, R. Zulli, M.L. Muiesan, E. Agabiti-Rosei, Cardiovascular status of carriers of the apolipoprotein A-I(Milano) mutant: the Limone sul Garda study, Circulation 103 (2001) 1949–1954.
[48] E.T. Alexander, M. Tanaka, M. Kono, H. Saito, D.J. Rader, M.C. Phillips, Structural and functional consequences of the Milano mutation (R173C) in human apolipoprotein A-I, J. Lipid Res. 50 (2009) 1409–1419.
[49] G.L. Weibel, E.T. Alexander, M.R. Joshi, D.J. Rader, S. Lund-Katz, M.C. Phillips, G.H. Rothblat, Wild-type ApoA-I and the Milano variant have similar abilities to stimulate cellular lipid mobilization and efflux, Arterioscler. Thromb. Vasc. Biol. 27 (2007) 2022–2029.
[50] L. Zhu, J. Petrlova, P. Gysbers, H. Hebert, S. Wallin, C. Jegerschöld, J.O. Lagerstedt, Structures of apolipoprotein A-I in high density lipoprotein generated by electron microscopy and biased simulations, Biochim. Biophys. Acta (2017), http://dx.doi.org/10.1016/j.bbagen.2017.07.017.
[51] M.N. Oda, M.S. Budamagunta, M.S. Borja, J. Petrlova, J.C. Voss, J.O. Lagerstedt, The secondary structure of apolipoprotein A-I on 9.6-nm reconstituted high-density lipoprotein determined by EPR spectroscopy, FEBS J. 280 (2013) 3416–3424.